CRYSTAL GROWTH & DESIGN

Subscriber access provided by READING UNIV

Article

A semiconducting copper(II) Metal–Organic Framework with (4,4) square grid topology: Synthesis, characterization and application in the formation of a photo-switch

Samim Khan, Soumi Halder, Partha Pratim Ray, Santiago Herrero,
Rodrigo Gonzalez-Prieto, Michael G. B. Drew, and Shouvik Chattopadhyay

Cryst. Growth Des., **Just Accepted Manuscript** • DOI: 10.1021/acs.cgd.7b00830 • Publication Date (Web): 12 Dec 2017

Downloaded from http://pubs.acs.org on December 14, 2017

Just Accepted

"Just Accepted" manuscripts have been peer-reviewed and accepted for publication. They are posted online prior to technical editing, formatting for publication and author proofing. The American Chemical Society provides "Just Accepted" as a free service to the research community to expedite the dissemination of scientific material as soon as possible after acceptance. "Just Accepted" manuscripts appear in full in PDF format accompanied by an HTML abstract. "Just Accepted" manuscripts have been fully peer reviewed, but should not be considered the official version of record. They are accessible to all readers and citable by the Digital Object Identifier (DOI®). "Just Accepted" is an optional service offered to authors. Therefore, the "Just Accepted" Web site may not include all articles that will be published in the journal. After a manuscript is technically edited and formatted, it will be removed from the "Just Accepted" Web site and published as an ASAP article. Note that technical editing may introduce minor changes to the manuscript text and/or graphics which could affect content, and all legal disclaimers and ethical guidelines that apply to the journal pertain. ACS cannot be held responsible for errors or consequences arising from the use of information contained in these "Just Accepted" manuscripts.

ACS Publications

Crystal Growth & Design is published by the American Chemical Society. 1155 Sixteenth Street N.W., Washington, DC 20036

Published by American Chemical Society. Copyright © American Chemical Society. However, no copyright claim is made to original U.S. Government works, or works produced by employees of any Commonwealth realm Crown government in the course of their duties.

A semiconducting copper(II) Metal–Organic Framework with (4,4) square grid topology: Synthesis, characterization and application in the formation of a photo-switch

Samim Khan[a], Soumi Halder[b], Partha Pratim Ray[b], Santiago Herrero[c], Rodrigo González-Prieto[c], Michael G. B. Drew[d] and Shouvik Chattopadhyay[a,*]

[a] *Department of Chemistry, Inorganic Section, Jadavpur University, Kolkata – 700 032, India. e-mail: shouvik.chem@gmail.com*

[b] *Department of Physics, Jadavpur University, Kolkata 700032, India.*

[c] *Departamento de Química Inorgánica, Facultad de Ciencias Químicas, Universidad Complutense de Madrid, Ciudad Universitaria, 28040 Madrid, Spain.*

[d] *School of Chemistry, The University of Reading, P.O. Box 224, Whiteknights, Reading RG6 6AD, UK.*

Abstract

A phenoxo and end-to-end thiocyanate bridged copper(II) MOF, $[Cu_2L_2(\mu\text{-}1,3\text{-}SCN)_2]_n$, where HL is an potential tetradentate N_2O_2 donor Schiff base ligand, 2-(2-(ethylamino)ethylimino)methyl)-6-ethoxyphenol, has been synthesized and characterized. The band gap, bulk capacitance, electron lifetime, relaxation time, dielectric constant and DC conductivity of the complex in the solid state have been studied. Variable temperature magnetic susceptibility measurement indicates the presence of weak antiferromagnetic interactions among the copper (II) centres with J= -0.97 cm^{-1}. The complex shows increase in conductivity when illuminated with visible light (photosensitivity ~2.833).

Keywords: Copper(II); photo-sensitive, antiferromagnetic, band gap, DC conductivity, bulk capacitance, dielectric constant

Introduction

The metal ions are denoted as nodes and ligands as linkers in multidimensional metal–organic frameworks (MOFs).[1-3] An appropriate metal–ligand complex could also be regarded as node in place of a bare metal ion.[4-5] The significance of the synthesis and characterization of these MOFs lies in their promising potential applications as functional materials.[6-8] Focusing to copper(II), varieties of copper(II)-MOFs are synthesized by various groups in order to understand the structural and chemical factors that govern the exchange coupling between paramagnetic copper(II) centres and also for developing new functional molecular-based materials.[9-11] A variety of bridging groups have been employed for the synthesis of such systems; among them the phenoxo oxygen atom of the salicylaldehyde derived Schiff bases deserves a special mention.[12-13] The magnetic properties (i.e. J values of the spin coupling) of only phenoxo-bridged complexes containing the Cu_2O_2 cores have been postulated to be dependent upon various factors, such as the coordination geometry of the copper ions, the Cu–O–Cu angle, the Cu–O bond lengths, the Cu···Cu distances, Addison parameter, etc. The study of magnetic exchange mediated by this ligand is often complicated by the presence of additional bridging ligands,[14-17] e.g. pseudo-halide, which may bind adjacent copper(II) centres in end-on (EO) and end-to-end (EE) modes.[18] EO coordination mode of a pseudo-halide is associated with ferromagnetic or antiferromagnetic coupling depending on various other factors,[19-22] the EE pseudo-halide bridges, in general, propagate antiferromagnetic interactions,[23-25] although there is also a possibility of a ferromagnetic interaction between centres when the pseudo-halide binds in an end-to-end fashion.[26-27] The chemistry and magnetic properties of such complexes have been the subject of several reviews.[28-31] Interestingly, the dielectric property and conductivity of such complexes are relatively less explored. For example, the semiconducting nature of a cadmium(II) Schiff base complex having optical band gap values of 3.69 and 2.67 eV was characterized by the distribution of electronic states in both valence and conduction bands with the partial density of states.[32] The use of such complexes in light harvesting and energy transfer is also a promising area of research.

In present work, the photosensitivity of a synthesized semiconducting complex with a substantial on–off ratio has been demonstrated. Though several substances are reported to absorb visible light and generate photocurrent with a quick response, probably this is the first example of any coordination polymer constructed by copper(II) Schiff base complex and characterized by single crystal X-ray crystallography. Herein, we would like to report the synthesis and X-ray characterization of a novel 2D coordination polymer having copper(II) Schiff base building block. The optical band gap of the complex in the solid state has been estimated experimentally. The bulk capacitance, electron lifetime, relaxation time and dielectric constant of the complex were also explored. The value of photosensitivity is calculated to be 2.833. The complex shows increase in conductivity from 3.63×10^{-5} Scm^{-1} to 4.13×10^{-5} Scm^{-1} in presence of light.

Results and discussion

Synthesis

The potential tetradentate Schiff base ligand, HL, was prepared by the condensation of N-ethyl-1,2-diaminoethane with 3-ethoxysalicylaldehyde following the literature method.[33-35] The potential tetradentate Schiff base, HL, acted as a tridentate ligand and occupied three sites of the octahedral copper(II). The remaining sites were occupied by one nitrogen and one sulpher atoms from two end to end bridged thiocyanates and one phenoxo oxygen from a different ligand to form a two-dimensional coordination polymer, $[Cu_2L_2(\mu\text{-}1,3\text{-}SCN)_2]_n$ was formed. The formation of the complex is shown in scheme 1.

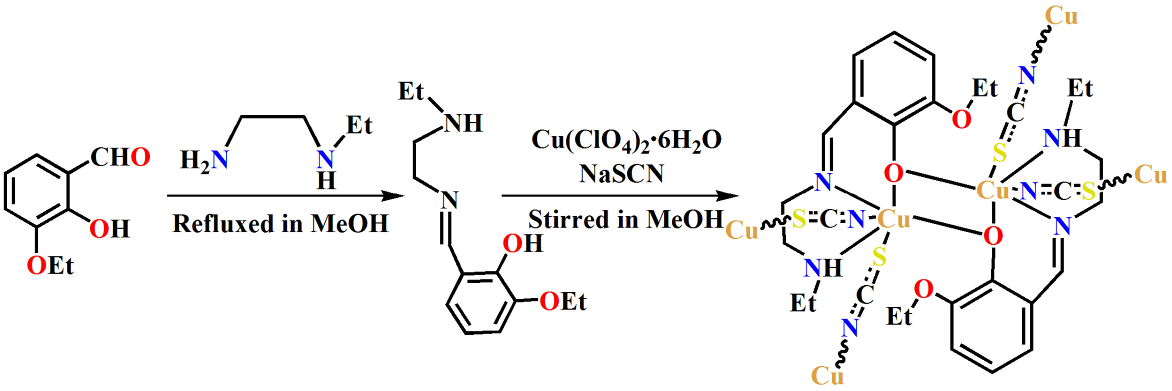

Scheme **1:** Synthetic route to the complex.

Description of structure

The complex crystallizes in the orthorhombic space group, *Pbca*. The structure determination reveals that the copper(II) centre is coordinated by one amine nitrogen atom, N(22), one imine nitrogen atom, N(19), one phenoxo oxygen atom, O(11), of the deprotonated Schiff base ligand, $(L)^-$, and one nitrogen atom, N(1) and one sulfur atom, S(1) of two end-to-end bridging thiocyanate ligands. The sixth coordination site is occupied by a symmetry related (1-x,-y,1-z) phenoxo oxygen atom, $O(11)^a$, from a Schiff base ligand to complete its octahedral geometry. The symmetry related phenoxo oxygen, $O(11)^a$ connect two copper(II) to form a pseudo-dimer (Fig. 1). The pseudo-dimeric bridging unit Cu_2O_2 describes a rhombohedral plane.

The rhombohedral angles of O(11)-Cu(1)-O(11)^{a}, Cu(1)-O(11)^{a}-Cu(1)^{a}, O(11)^{a}-Cu(1)^{a}-O(11), Cu(1)^{a}-O(11)-Cu(1) are 91.78(11), 88.2(1), 91.8(1) and 88.2(1)^{o} respectively. The saturated five member ring, Cu(1)–N(22)–C(21)–C(20)–N(19) presents an envelope conformation with puckering parameters q(2) = 0.409(5) and φ = 108.0(5)^{o}.[36] Selected bond angles are presented in Table S1 (Supporting Information). Each copper(II) center of the pseudo-dimer is connected to two neighboring copper(II) centers of two different pseudo-dimers through two end-to-end thiocyanate bridges to form a two-dimensional polymeric layer along crystallographic ab plane (Fig. 2a). Topology analysis reveals a (4,4)-square grid topology (Fig. 2b) with copper(II) occupying the nodes, where end-to-end thiocyanate connectors take part in the formation of edges.

The complex shows intra-pseudo-dimeric hydrogen bonding (Fig. S1, Supporting Information). The hydrogen atom, H(22), attached to the nitrogen atom, N(22), is participated in hydrogen bonding interaction (Table S2, Supporting Information) with the symmetry-related oxygen atom, O(13)^{a} {symmetry transformation ^{a} = 1-x,-y,1-z }. The methyl hydrogen atom, H(11D), attached to C(112), is involved in significant C–H···π interaction (Table S3, Supporting Information) with the symmetry related (3/2-x,-1/2+y,z) phenyl ring C(12)-C(13)-C(14)-C(15)-C(16)-C(17). As the complex consists of centrosymmetric pseudo-dimeric building block, each interaction is duplicated and the combination of these interactions creates a 2-D supramolecular structure (Fig. S2, Supporting Information).

Powder X-ray diffraction

The experimental PXRD pattern of the bulk product is in good agreement with the simulated XRD pattern from single-crystal X-ray diffraction, indicating consistency of the bulk sample (Fig. 3).

Hirshfeld surfaces

The Hirshfeld surfaces of the complex, mapped over d_{norm}, shape index and curvedness, are illustrated in Fig. S3, Supporting Information. 2D fingerprint plots are shown in Fig. 4, where intermolecular interactions appear as distinct spikes. Decomposition of fingerprint plots able us to highlight particular atom pair close contacts.[37] The proportion of C···H/H···C interaction comprises 15.6%, where as O···H/H···O interaction comprises 6.1% of the Hirshfeld surfaces for each molecule.

IR and electronic spectra

In the IR spectrum of the complex, a band corresponding to the azomethine (C=N) stretching vibration appears at 1649 cm^{-1}.[38] The μ-1,3 bridging mode of the thiocyanate group is confirmed by the splitting of the absorption band corresponding to the $\gamma_{C=N}$ asymmetric stretching that appears at 2102 and 2075 cm^{-1} indicates the S- and N-coordination modes of the thiocyanate ligand respectively.[39] Two medium bands at 846 and 749 cm^{-1} may be assigned to υ(CS).[40] The bands in the range of 2968-2865 cm^{-1} are assigned due to alkyl C-H bond stretching vibrations.[41] A moderately strong, sharp peak at 3230 cm^{-1}, may be assigned to N–H stretching vibration.[42]

The intense absorption bands at 276 and 372 nm may be assigned as intraligand π–π* and ligand to metal charge transfer (LMCT) transitions respectively.[43] The absorption band in the visible range at 682 nm (Fig. 5) may be assigned as d–d transition.[44]

Morphology

The FESEM image of the material is presented in Fig. S4 (Supporting Information) which shows that the material has an arbitrary morphology.

Mass spectra

The electrospray ionization mass spectra (ESI-MS positive) are performed to determine molecular weight and study fragmentation pattern of possible complex adduct. The ESI-MS positive spectrum of the complex is recorded in acetonitrile solution and the result is shown in Fig. S5. In the mass spectrum of complex, the peak at m/z = 356.05 may be assigned to $[CuL(SCN)H]^+$ and the peak at m/z = 298.07 corresponds to the presence of monopositive $[Cu(L)]^+$.

Cyclic voltammetry

The cyclic voltammogram of the complex shows an oxidation peak (E_{pa}) at about the potential 1332 mV. This can be assigned as Cu^{II}/Cu^{III} oxidation process. A wave (E_{pc}) at 1265 mV is observed during the reverse scan (Fig. 6). The difference between the cathodic and anodic peak is 67 mV for the complex, and this suggests the reversible nature of the electron transfer processes. $E_{1/2}$ is calculated as the average of anodic (E_{pa}) and cathodic (E_{pc}) peak potentials. The value of $E_{1/2}$ is 1.3 V. The criteria of reversibility were checked by observing the constancy of the peak–peak separation ($\Delta E_p = E_{pa}-E_{pc}$) and the ratio of peak heights ($i_{pa}/i_{pc} \sim 1$) with variation of scan rates. The redox signal remains virtually invariant under different scan rates (0.01–1.0 Vs^{-1}) in the temperature range 300–280 K. Any solvent dependent shifts and changes in the electrochemical reversibility of the redox couples are not noteworthy. Other peaks at negative potentials may be due to the reduction to lower oxidation states of copper.

Band gap measurement

The absorption spectra recorded is shown in the inset of Fig. 7. The spectra show absorption in the visible region with absorption band edge at around 420 nm. The optical band gap energy (E_g) of the complex was evaluated using the Tauc's equation[45]

Error! Reference source not found.

(1)

Where 'α' is the absorption coefficient, 'E_g' is the band gap, 'h' is Planck's constant , 'γ' is the frequency of light and the exponent 'n' is the electron transition process constant. 'A' is the constant which is taken 1 for ideal case. To calculate the optical band gap energy, the value of n is taken as ½ (The proof is given along with Fig. S6 in Supporting Information).

The Tauc's plot of the complex is given in Fig. 7. The optical energy band gap (E_g) can be determined by extrapolating the linear region of the plot of (αh**Error! Reference source not found.**)^2 vs. hγ to α=0 absorption and the value is estimated to be about 2.95 eV. We tried to perform the calculations of the crystal lattice within the Generalized-Gradient approximation (GGA) and the Perdew-Burke-Ernzerhof (PBE) formulation for the exchange-correlation functional. However, the presence of strong hybridization between the Cu 3d and N 2p orbitals leads to the formation of isolated and intermediate bands in the crystal band gap. Therefore, theoretical band gap in it cannot be determined.

The light absorption of the material in visible region indicate that the material has some light induced properties and the optical band gap also suggests that there is semiconducting nature which encourages us to further investigate the dielectric properties of the synthesized material.

Dielectric parameters

The dielectric parameters were measured on pellet. The synthesized complex was pelletized into a disc form of diameter 7.32 mm and thickness 1.8 mm.

The complex plane impedance plot i.e. Nyquist plot of the sample is shown in Fig. 8a. The plot shows a semicircle where the bulk resistance is evaluated from the diameter of the arc.

The Bode plot of the complex has been shown in Fig. 8b and the electron lifetime of the material was calculated. The peak frequency is related to the inverse of the recombination lifetime or electron lifetime. Electron lifetime is determined from the following equation[46]

$$\tau_n = \frac{1}{2\pi f_{min}} \qquad (2)$$

Here τ_n is the electron lifetime and f_{min} is the peak frequency.

The impedance loss spectrum of the complex is represented in Fig. S7, Supporting Information. It is used to determine the relaxation time of the complex[47] using the following equation.

$$\tau = \frac{1}{2\pi f_p} \qquad (3)$$

τ is the relaxation time and f_p is the peak frequency determined from the graph.

Fig. S7, ESI gives the curve showing the variation of the capacitance (C) as a function of the frequency (f) at constant bias potential. The room temperature capacitance of the complex shows frequency dependence at relatively low frequencies. The capacitance decreases with the increase in frequency and becomes saturated at higher frequency (Fig. S8, Supporting

Information). Using the value of capacitance at the saturation level the dielectric constant of the complex was calculated using the following equation[45]:

$$\varepsilon_r = \frac{1}{\varepsilon_0} . \frac{C.d}{A} \qquad (4)$$

Where, ε_0 is the permittivity of free space, ε_r is the dielectric constant of the synthesized material, C is the capacitance (at saturation) and d and A are the thickness and effective area of the pellet respectively. Using the above formula the dielectric constant (**Error! Reference source not found.**) of the material was estimated and given in Table 2.

The above electrical parameters and the obtained band gap value indicate that the synthesized product has a semiconducting nature. Hence, we have further studied its light sensing behaviour to check the suitability of the synthesized material for electronic application.

Magnetic properties

The experimental $\chi_M T$ value at room temperature (0.86 $cm^3 \cdot mol^{-1}$) for the complex corresponds to the presence of two independent copper(II) centres in the molecule (0.75 $cm^3 \cdot mol^{-1}$ considering $g = 2$) indicating an almost negligible interaction between the copper(II) centres. However, although this value remains practically constant until around 50 K, then decreases slowly and finally drops at 11 K, reaching a value of 0.54 $cm^3 \cdot mol^{-1}$ at 2K (Fig. 9). This decrease at very low temperatures indicates a small antiferromagnetic interaction between copper(II) atoms. Therefore, the magnetic behaviour of this complex has been simulated using equation 5:

$$\chi = \frac{Ng^2\mu_B^2}{kT} \times \frac{2e^{\frac{2J}{kT}}}{1+3e^{\frac{2J}{kT}}} + TIP \qquad (5)$$

Equation 5 was derived by Bleaney and Bowers[48] from the Hamiltonian $H = -2J_{ij}S_iS_j$. A term considering a temperature independent paramagnetism (*TIP*) has also been included.

The fit of the experimental data using equation 5 yields the following values: $g = 2.14$; $J = -0.97$ cm^{-1}, $TIP = 2.29\text{x}10^{-5}$ cm^3 mol^{-1}, with $\sigma^2 = 9.71\text{x}10^{-5}$. In the equation 5, the interactions between copper(II) pseudo-dimers have not been considered despite that this type of interactions could influence notably the magnetic behaviour of the compounds even through hydrogen bonds.[49] The introduction of one term to consider the interdimer interactions using the molecular field approximation[50] does not improve the fits showing a *J* value of the same order. Therefore, the interdimer coupling in this complex seems to be negligible.

It is well known that bis(μ-phenoxo)-bridged dinuclear copper(II) complexes show magnetic properties strongly dependent on structural factors. The Cu-O-Cu bridging angle, the out-of-plane shift of the phenyl rings, the Cu-O bond length, the planarity of the Cu_2O_2 core, and the conformation and rotation of the phenyl groups can influence the magnetic behaviour of this type of complexes. Although the majority of them show very strong antiferromagnetic coupling constants (up to $2J = -905$ cm^{-1}), small changes in these geometric parameters can make some of the complexes present only weak antiferromagnetic, or even ferromagnetic, intradimer interactions.[15,31,51-55]

The Cu-O-Cu bridging angle is one of the main parameters affecting these magnetic properties. Thompson and *col.*[52] found that the antiferromagnetic coupling increased linearly with the increment of this angle for flat macrocyclic dinuclear copper(II) complexes derived from 2,6-di(R)formylphenols. This tendency is similar to those described by Ruiz *et al.*[56] for similar hydroxo- and alkoxo-bridged compounds. However, these later complexes show weaker antiferromagnetic couplings and even ferromagnetic for small Cu-O-Cu angles, while flat macrocyclic phenoxo-bridged complexes show antiferromagnetic interactions in a broad range of angles.[52,56] High values of the out-of-plane angle (τ) of the phenyl rings, *i.e.* when the phenyl groups are not in the Cu_2O_2 plane, favour the ferromagnetic contributions.[31, 53,56,58] However, this parameter has more influence in the variation of the coupling constants when the phenyl rings of the phenoxo ligands present a *syn* conformation.[31,53] In this case the antiferromagnetic coupling is enhanced for values of τ in the range 0 – 20° whereas the contrary occurs for $\tau > 20°$. On the contrary, the out-of-plane angle does not have a very important effect if the phenyl rings show an *anti* conformation, although the ferromagnetic contribution is slightly favoured for high values of τ. Also, the rotation of the phenyl rings influences the magnetic coupling, since the antiferromagnetic interactions increase with a perpendicular orientation of the ring with respect to the Cu_2O_2 core. [31] Giapintzakis, and *col.*[52] have also reported an important correlation of the magnetic coupling with the $Cu\text{-}O_{phenolate}$ bond length. Distances lower than 1.98 Å are associated to strong antiferromagnetic coupling constants, whereas bond lengths higher than 1.98 Å can show either weak antiferromagnetic or ferromagnetic behaviour. Deviations from the planarity of the Cu_2O_2 framework, as a function of the Cu-O-Cu-O torsion angle, have also been studied for these complexes[31] and for the analogous hidroxo-bridged complexes.[57] High torsion angles reduce the antiferromagnetic couplings and favour the ferromagnetic contribution. Although in copper(II) dimers with pentacoordinate environment, the magnetic exchange can be influenced by the type of connection, such as axial-equatorial,[15,51,54] basal-basal,[15,54] or basal-apical,[54,58] this variable is not considered for octahedral environments.

Therefore, a magneto-structural analysis can be used to explain the weak antiferromagnetic intradimer interaction (J = -0.97) cm^{-1} found for the complex. First of all, its

Cu-O-Cu bridging angle (88.22°) is very low. Although experimental values are found in a wide range (85.5-110.4°), most of them are in the 95-110.4° range.[31] In addition, the τ value (45.06°) is high and the Cu-$O_{phenolate}$ distances are long (2.347 Å, in average). All those values are consistent with very weak antiferromagnetic or even ferromagnetic coupling. Moreover, the *anti* conformation of the phenyl groups for such a high value of τ makes weaker the antiferromagnetic coupling. Nevertheless, there are other structural parameters that favour antiferromagnetic coupling and, consequently, avoid reaching the ferromagnetic interactions: the phenyl rings are almost perpendicular to the Cu_2O_2 core, which is completely flat (the Cu-O-Cu-O torsion angle is 0°). As a result of all these factors, the complex has very weak antiferromagnetic coupling. Nevertheless, the existence of weak ferromagnetic interaction through the phenoxo group and weak interdimers antiferromagnetic interactions through the thiocyanate ligands cannot be discarded.

Electrical properties

The presence of strong absorbance of the synthesized complex in the visible wavelength region of light suggests that incident radiation has some influence on the charge transport properties. Furthermore the value of optical band gap indicated semiconducting nature of the complex. To elucidate charge transport mechanism, electrical current was measured at a bias voltage of 2V.

The transient photocurrent response shown in Fig. 10 is generated by the transfer of excited photoelectrons from the highest occupied molecular orbital (HOMO) to the lowest unoccupied molecular orbital (LUMO). The transient photocurrent responses of the complex are investigated for several on-off cycles of irradiations. As shown in Fig. 10, the current falls rapidly to the initial value when illumination turns off. Photocurrent again goes back to the maximum value as soon as the light turns on. This characteristic behaviour depicts that most of the photogenerated electrons reach the ITO coated substrate to produce photocurrent under the irradiation of visible light. The result suggests that photogenerated electron–hole pairs separated efficiently for the complex. The photosensitivity of the material is 2.833 which is determined from Fig. 10. This figure also tells that the material is very stable under the exposure of light. The conductivity was measured from the current-voltage characteristics graph and it was estimated as 3.63 x 10^{-5} Scm^{-1} and 4.13 x 10^{-5} Scm^{-1} under dark and light conditions. The electrical transport parameters which are detrimental to device performance suggest that this material can be a promising candidate for photo-switch.

Conclusion

In conclusion, we report the synthesis and X-ray characterization of a novel coordination polymer based on a N_2O_2 donor potential tetradentate Schiff base ligand and μ-1,3-thiocyanates as linkers. The copper(II) MOF exhibit electrical conductivity that has been rationalised by band gap measurement. The phenoxo bridged complex has very weak antiferromagnetic coupling. Several dielectric parameters like bulk capacitance, electron lifetime, relaxation time and dielectric constant of the complex in the solid state have also been studied. On irradiation with visible light, there is a considerable increase in the conductivity of the present complex. The photosensitivity of the material is 2.833 and the material is very stable under the exposure of light which suggests that it can be used as photo-switch.

Supporting Information

Details experimental section, Theoretical methods, Hirshfeld Surfaces, Data Tables of bond angles, hydrogen bond, C-H···π interactions (Table S1–S3); hydrogen bond, C-H···π interactions (Fig. S1 to Fig. S2); Hirshfeld surfaces, FESEM image, ESI-MS (Fig. S3 to Fig. S5); Plot of d[ln(αhν)]/d(hν) vs. hν and plot of ln(αhν) vs. ln(hν-E_g) (Fig. S6); Impedance loss spectrum, capacitance versus frequency graph (Fig. S7 to Fig. S8).

Accession Codes

CCDC 1542881 contains the supplementary crystallographic data for this paper. These data can be obtained free of charge via www.ccdc.cam.ac.uk/data_request/cif, or by emailing data_request@ccdc.cam.ac.uk, or by contacting The Cambridge Crystallographic Data Centre, 12, Union Road, Cambridge CB2 1EZ, UK; fax: +44 1223 336033.

Acknowledgments

Financial support received from the Spanish Ministerio de Economíay Competitividad (CTQ2015-63858-P, MINECO/FEDER) is gratefully acknowledged. PPR acknowledges UPE programme of University Grants Commission and FIST programme of Department of Science and Technology, Govt. of India.

References

1. Bai, Y.; Dou, Y.-B.; Xie, L.-H.; Rutledge, W.; Li, J.-R.; Zhou, H.-C. Zr-based metal-organic frameworks: design, synthesis, structure, and applications. *Chem. Soc. Rev.* **2016**, *45*, 2327−2367.

2. Huang, Y.-Q.; Wan, Y.; Chen, H.-Y.; Wang, Y.; Zhao, Y.; Xiaoa, X.-F. Construction of metal–organic coordination networks with various metal-linker secondary building units: structures and properties. *New J. Chem.* **2016**, *40*, 7587−7595.

3. Yaghi, O. M.; O'Keeffe, M.; Ockwig, N. W.; Chae, H. K.; Eddaoudi, M.; Kim, J. Reticular synthesis and the design of new materials. *Nature* **2003**, *423*, 705–714.

4. Guillerm, V.; Kim, D.; Eubank, J. F.; Luebke, R.; Liu, X.; Adil, K.; Lah, M. S.; Eddaoudi, M. A supermolecular building approach for the design and construction of metal−organic frameworks. *Chem. Soc. Rev.* **2014**, *43*, 6141−6172.

5. Schoedel, A.; Li, M.; D. Li.; O'Keeffe, M.; Yaghi, O.M. Structures of Metal−Organic Frameworks with Rod Secondary Building Units. *Chem. Rev.* **2016**, *116*, 12466–12535.

6. Furukawa, H.; Cordova, K. E.; O'Keeffe, M.; Yaghi, O. M. The chemistry and applications of metal-organic frameworks. *Science*, **2013**, *341*, 1230444.

7. Rodenas, T.; Luz, I.; Prieto, G.; Seoane, B.; Miro, H.; Corma, A.; Kapteijn, F.; Llabres i Xamena, F. X.; Gascon, J. Metal ́ −Organic Framework Nanosheets in Polymer Composite Materials for Gas Separation. Nat. Mater. **2014**, *14*, 48−55.

8. Yang, Y.; Wang, F.; Yang, Q.; Hu, Y.; Yan, H.; Chen, Y. Z.; Liu, H.; Zhang, G.; Lu, J.; Jiang, H. L.; Xu, H. Hollow Metal-Organic Framework Nanospheres Via Emulsion-Based Interfacial Synthesis and Their Application in Size-Selective Catalysis. *ACS Appl. Mater. Interfaces.* **2014**, *6*, 18163−18171.

9. Senchyk, G. A.; Lysenko, A. B.; Rusanov, E. B.; Chernega, A. N.; Jezierska, J.; Domasevitch, K. V.; Ozarowski, A. Structure and Magnetic Behavior of Cu^{II} MOFs Supported by 1,2,4-Triazolyl-Bifunctionalized Adamantane Scaffold. *Eur. J. Inorg. Chem.* **2012**, 5802−5813.

10. Vasylevs'kyy, S. I.; Senchyk, G. A.; Lysenko, A. B.; Rusanov, E. B.; Chernega, A. N.; Jezierska, J.; Krautscheid, H.; Domasevitch, K. V.; Ozarowski, A. 1,2,4-Triazolyl-Carboxylate-Based MOFs Incorporating Triangular Cu(II)-Hydroxo Clusters: Topological Metamorphosis and Magnetism. *Inorg. Chem.* **2014**, *53*, 3642−3654.

11. Wang, C.; Liu, D.; Lin, W. Metal−Organic Frameworks as A Tunable Platform for Designing Functional Molecular Materials. *J. Am. Chem. Soc.* **2013**, *135*, 13222−13234.

12. Hussain, N.; Bhardwaj, V. K. The influence of different coordination environments on one-dimensional Cu(II) coordination polymers for the photo-degradation of organic dyes. *Dalton Trans.* **2016**, *45*, 7697−7707.

13. Mukherjee, S.; Mukherjee, P. S. Cu^{II}–azide polynuclear complexes of Cu_4 building clusters with Schiff-base co-ligands: synthesis, structures, magnetic behavior and DFT studies. *Dalton Trans.* **2013**, *42*, 4019-4030.

14. Biswas, A.; Das, L. K.; Drew, M. G. B.; Aromí, G.; Gamez, P.; Ghosh, A. Insertion of a Hydroxido Bridge into a Diphenoxido Dinuclear Copper(II) Complex: Drastic Change of the Magnetic Property from Strong Antiferromagnetic to Ferromagnetic and Enhancement in the Catecholase Activity. *Inorg. Chem.* **2012**, *51*, 7993−8001.

15. Biswas, A.; Drew, M. G. B.; Ribas, J.; Diaz, C.; Ghosh, A. Synthesis, Crystal Structures and Magnetic Properties of a Phenoxo-Bridged Dinuclear Cu^{II} Complex and a Dicyanamide Bridged Novel Molecular Rectangle Based on It. *Eur. J. Inorg. Chem.* **2011**, 2405−2412.

16. Hay, J. P.; Thibeault, J. C.; Hoffmann, R. Orbital interactions in metal dimer complexes. *J. Am. Chem. Soc.* **1975**, *97*, 4884−4899.

17. Bikas, R.; Monfared, H. H.; Vasylyeva, V.; Sanchiz, J.; Alonso, J.; Barandiaran, J. M.; Janiak, C. Synthesis, structure, magnetic properties and EPR spectroscopy of a copper(II) coordination polymer with a ditopic hydrazone ligand and acetate bridges. *Dalton Trans.* **2015**, *43*, 11925–11935.

18. Naiya, S.; Biswas, C.; Drew, M. G. B.; Gomez-García, C. J.; Clemente-Juan, J. M.; Ghosh, A. A Unique Example of Structural and Magnetic Diversity in Four Interconvertible Copper(II)-Azide Complexes with the Same Schiff Base Ligand: A Monomer, a Dimer, a Chain, and a Layer. *Inorg. Chem.* **2010**, *49*, 6616−6627.

19. Fadaee, F.; Amirnasr, M.; Prsa, K.; Pattison, P.; Shaik, N. E.; Rønnow, H. M.; Esrafili, M. D.; Omrani, A.; Amiri, A.; Schenk-Joß, K. Intrachain anti-ferromagnetic exchange in a 1D branched-chain built of two different copper(II) centres interlinked by end-on azido and phenoxo bridges: electron density map, electrochemical and magnetic properties. *RSC Adv.* **2015**, *5*, 59926−59934.

20. Chaudhuri, P.; Wagner, R.; Weyhermuller, T. Ferromagnetic vs Antiferromagnetic Coupling in Bis(μ-phenoxo)dicopper(II) Complexes. Tuning of the Nature of Exchange Coupling by Remote Ligand Substituents. *Inorg. Chem.* **2007**, *46*, 5134–5136.

21. Koner, S.; Saha, S.; Mallah, T.; Okamoto, K.-I. Unprecedented Low Cu−N(azide)−Cu Angles in End-On Double Azido Bridged Copper(II) Complex. *Inorg. Chem.* **2004**, *43*, 840–842.

22. Jana, S.; Shaw, B. K.; Bhowmik, P.; Harms, K.; Drew, M. G. B.; Chattopadhyay, S.; Saha, S. K. Field-Induced Ferromagnetism and Multiferroic Behavior in End-on Pseudohalide-Bridged Dinuclear Copper(II) Complexes with Tridentate Schiff Base Blocking Ligands. *Inorg. Chem*. **2014**, *53*, 8723-8734.

23. Grove, H.; Julve, M.; Lloret, F.; Kruger, P. E.; Törnroos, K. W.; Sletten, J. Syntheses, crystal structures and magnetic properties of copper(II) polynuclear and dinuclear compounds with 2,3-bis(2-pyridyl)pyrazine (dpp) and pseudohalide as ligands. *Inorg. Chim. Acta* **2001**, *325*, 115-124.

24. Triki, S.; Gomez-García, C. J.; Ruiz, E.; Sala-Pala, J. Asymmetric Azido−Copper(II) Bridges: Ferro- or Antiferromagnetic? Experimental and Theoretical Magneto−Structural Studies. *Inorg. Chem.* **2005**, *44*, 5501−5508.

25. Carranza, J.; Brennan, C.; Sletten, J.; Lloret, F.; Julve, M. Three one-dimensional systems with end-to-end dicyanamide bridges between copper(II) centres: structural and magnetic properties. *J. Chem. Soc., Dalton Trans.* **2002**, 3164−3170.

26. Shaw, B. K.; Das, M.; Bhattacharyya, A.; Ghosh, B. N.; S. Roy.; Mandal, P.; Rissanen, K.; Chattopadhyay, S.; Saha, S. K. Field-induced ferromagnetism due to magneto-striction in 1-D helical chains. *RSC Adv.* **2016**, *6*, 22980–22988.

27. Bhattacharyya, A.; Ghosh, B. N.; Rissanen, K.; Aparicio. J. R.; Chattopadhyay, S. Formation of a novel ferromagnetic end-to-end cyanate bridged homochiral helical copper(II) Schiff base complex via spontaneous symmetry breaking. *Dalton Trans.* **2015**, *44*, 493–497.

28. Melnik, M. Study of the relation between the structural data and magnetic interaction in oxo-bridged binuclear copper(II) compounds. *Coord. Chem. Rev.* **1982**, *42*, 259–293.

29. Batten, S. R.; Murray, K. S. Structure and magnetism of coordination polymers containing dicyanamide and tricyanomethanide. *Coord. Chem. Rev.* **2003**, *246*, 103−130.

30. Adhikary, C.; Koner, S. Structural and magnetic studies on copper(II) azido complexes. *Coord. Chem. Rev.* **2010**, *254*, 2933–2958.

31. Venegas-Yazigi, D.; Aravena, D.; Spodine, E.; Ruiz, E.; Alvarez, S. Structural and electronic effects on the exchange interactions in dinuclear bis(phenoxo)-bridged copper(II) complexes. *Coord. Chem. Rev.* **2010**, *254*, 2086−2095.

32. Roy, S.; Dey, A.; Ray, P. P.; Castro, J. O.; Frontera, A.; Chattopadhyay, S. Application of a novel 2D cadmium(II)-MOF in the formation of a photo-switch with a substantial on–off ratio. *Chem. Commun.* **2015**, *51*, 12974-12976.

33. Bhattacharyya, A.; Bhaumik, P. K.; Jana P. P.; Chattopadhyay, S. Anion mediated diversity in the nuclearity of nickel(II) complexes with a N_2O donor Schiff base: Formation of a supra-molecular chain via Br···Br interactions. *Polyhedron*, **2014**, *78*, 40-45.

34. Das, M.; Harms, K.; Chattopadhyay, S. Novel tandem synthesis of bis(μ-NN'-tetrazolate) bridged dinuclear nickel(II) Schiff base complex via [3 + 2] cyclo-addition at ambient condition. *Dalton Trans*. **2014**, *43*, 5643-5647.

35. Bhattacharyya, A.; Harms, K.; Chattopadhyay, S. Formation of T4(1) water tapes interconnected via centrosymmetric nickel(II) Schiff base complex to produce a 3D architecture. *Inorg. Chem. Commun*. **2014**, *48*, 12-17.

36. Cremer, D.; Pople, J. A.; A General Definition of Ring Puckering Coordinates. *J. Am. Chem. Soc.* **1975**, *97*, 1354-1358.

37. Spackman, M. A.; Byrom, P. G.; Spackman, M. A.; Byrom, P. G.; A novel definition of a molecule in a crystal. *Chem. Phys. Lett.* **1997**, *267*, 215-220.

38. Khan, S.; Jana, S.; Drew, M. G. B.; Bauza, A.; Frontera, A.; Chattopadhyay, S. A novel method for copper(II) mediated region-selective bromination of aromatic rings under mild conditions. *RSC Adv.* **2016**, *6*, 61214–61220.

39. Thakurta, S.; Butcher, R. J.; Gomez-García, C. J.; Garribba, E.;´ Mitra, S. Synthesis, structural aspects and magnetic properties of an unusual 2D thiocyanato-bridged cobalt(II)–Schiff base network. *Inorg. Chim. Acta* **2010**, *363*, 3981−3986

40. Sabatini, A.; Bertini, I. Infrared Spectra between 100 and 2500 Cm^{-1} of Some Complex Metal Cyanates, Thiocyanates, and Selenocyanates. *Inorg. Chem.* **1965**, *4*, 959–961.

41. Roy, S.; Harms, K.; Chattopadhyay, S. Formation of three photoluminescent dinuclear cadmium(II) complexes with Cd_2O_2 cores. *Polyhedron* **2015**, *91*, 10-17.

42. Das, M.; Chatterjee, S.; Harms, K.; Mondal, T. K.; Chattopadhyay, S. Formation of bis(μ-tetrazolato)dinickel(II) complexes with N,N,O-donor Schiff bases via in situ 1,3-dipolar cyclo-additions: isolation of a novel bi-cyclic trinuclear nickel(II)–sodium(I)–nickel(II) complex. *Dalton Trans.* **2014**, *43*, 2936–2947.

43. Bhattacharyya, A.; Chattopadhyay, S. Spontaneous resolution of P and M helical copper(II) MOFs built from achiral precursors. *RSC Adv.* **2015**, *5*, 18252–18257.

44. Khan, S.; Masum, A. A.; Islam, M. M.; Drew, M. G. B.; Bauzá, A.; Frontera, A.; Chattopadhyay, S. Observation of π-hole interactions in the solid state structures of three new

copper(II) complexes with a tetradentate N_4 donor Schiff base: Exploration of their cytotoxicity against MDA-MB 468 cells. *Polyhedron* **2017**, *123*, 334–343.

45. Dey, A.; Middya, S.; Jana, R.; Das, M.; Datta, J.; Layek, A.; Ray, P. P.; Light induced charge transport property analysis of nanostructured ZnS based Schottky diode. *J Mater Sci: Mater Electron*, **2016**, *27*, 6325–6335.

46. Kern, R.; Sastrawan, R.; Ferber, J.; Stangl, R.; Luther, J. Modeling and interpretation of electrical impedance spectra of dye solar cells operated under open-circuit conditions. *J. Electrochim. Acta* **2002**, *47*, 4213−4225.

47. Barik, K. S.; Choudhary, R. N. P.; Singh, A. K.; Ac impedance spectroscopy and conductivity studies of Ba0.8Sr0.2TiO3 ceramics. *Adv. Mat. Lett.* **2011**, *2(6)*, 419-424.

48. Kahn, O. Molecular Magnetism, VCH, Weinheim, 1993, p. 104.

49. Ray, M. S.; Ghosh, A.; Bhattacharya, R.; Mukhopadhyay, G.; Drew, M. G. B.; Ribas, J. Different supramolecular hydrogen bond structures and significant changes in magnetic properties in dinuclear μ_2-1,1-N_3 copper(II) complexes with very similar tridentate Shiff base blocking ligands. *Dalton Trans.* **2004**, 252-259.

50. O'Connor, C.J. Magnetochemistry-Advances in Theory and Experimentation. *Prog. Inorg. Chem.* **1982**, *29*, 203–283.

51. Stylianou, M.; Drouza, C.; Viskadourakis, Z.; Giapintzakis, J.; Keramidas, A. D. Synthesis, structure, magnetic properties and aqueous solution characterization of *p*-hydroquinone and phenol iminodiacetate copper(II) complexes. *Dalton Trans.* **2008**, 6188-6204.

52. Thompson, L. K.; Mandal, S. K.; Tandon, S. S.; Bridson, J. N.; Park, M. K. Magnetostructural Correlations in Bis(μ2-phenoxide)-Bridged Macrocyclic Dinuclear Copper(II) Complexes. Influence of Electron-Withdrawing Substituents on Exchange Coupling. *Inorg. Chem.* **1996**, *35*, 3117-3125.

53. Biswas, A.; Drew, M. G. B.; Song, Y.; Ghosh, A. Effect of anionic co-ligands on structure and magnetic coupling of bis(μ-phenoxo)-bridged dinuclear copper(II) complexes. *Inorg. Chim. Acta* **2011**, *376*, 422-427.

54. Basak, S.; Sen, S.; Roy, P.; Gómez-García, C. J.; Hughes, D. L.; Butcher, R. J.; Garribba, E.; Mitra, S. Structural Variation and Magneto-Structural Correlation in Two New Dinuclear Bis(μ_2-Phenoxo)-Bridged Cu^{II} Schiff-Base Complexes: Catalytic Potential for the Peroxidative Oxidation of Cycloalkanes. *Aust. J. Chem.* **2010,** *63*, 479-489.

55. Archana V.; Imamura, Y.; Sakiyama, H.; Hada, M. Correlating Magnetic Exchange in Dinuclear Bis(phenolate)-Bridged Complexes: A Computational Perspective. *Bull. Chem. Soc. Jpn*. **2016**, *89*, 657-665.

56. Ruiz, E.; Alemany, P.; Alvarez, S.; Cano, J. Toward the Prediction of Magnetic Coupling in Molecular Systems: Hydroxo- and Alkoxo-Bridged Cu(II) Binuclear Complexes. *J. Am. Chem. Soc*. **1997**, *119*, 1297-1303.

57. Ruiz, E.; Alemany, P.; Alvarez, S.; Cano. J. Structural Modeling and Magneto-Structural Correlations for Hydroxo-Bridged Copper(II) Binuclear Complexes. *Inorg. Chem.* **1997**, *36*, 3683-3688.

58. Mashhun, A.; Zarei, S.A.; Piltan, M.; Chevreux, S.; Guillon, E. A binuclear copper(II) complex with diphenoxido-bridges: synthesis, characterisation, crystal structure and predicting the magnetic coupling constant. *J. Chem. Res.* **2016**, *40*, 114-119.

Table 1: Crystal data and refinement details of the complex.

Formula	$C_{14}H_{19}CuN_3O_2S$
Formula Weight	356.94
Temperature (K)	150
Crystal system	Orthorhombic
Space group	*Pbca*
a(Å)	13.3158(8)
b(Å)	10.3661(7)
c(Å)	22.9694(15)
Z	8

d_{calc} (g cm^{-3})	1.496
μ(mm^{-1})	1.516
F(000)	1480
Total Reflections	10650
Unique Reflections	4548
Observed data [I >2 σ (I)]	3108
No. of parameters	192
R(int)	0.062
R1, wR2 (all data)	0.1191, 0.1692
R1, wR2 [I > 2 σ (I)]	0.0797, 0.1549

Symmetry transformation ^{a} = 1-x,-y,1-z; ^{b} = 3/2-x,1/2+y,z.

Table 2: Dielectric parameters of the complex.

Complex	Bulk resistance	Bulk capacitance	Electron lifetime	Relaxation time	Dielectric constant
1	2.74 kΩ	6.59 x 10^{-11} F	1.59 x 10^{-8} sec	1.81 x10^{-7} sec	0.858

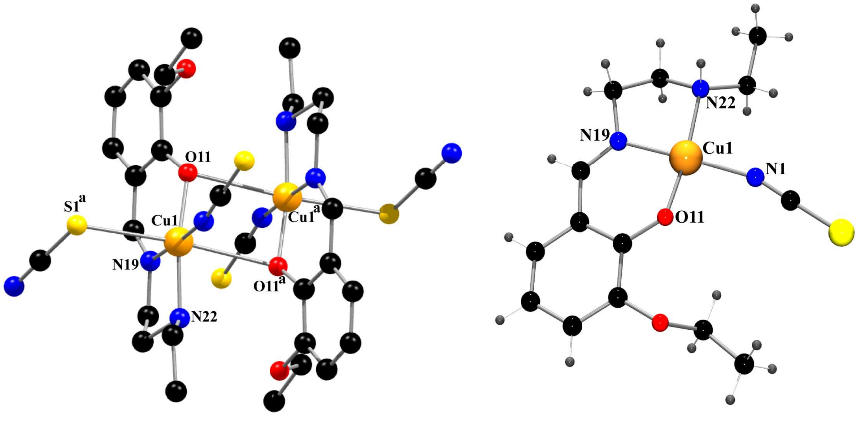

(a) (b)

Fig. 1: (a) Perspective view of the complex with selective atom-numbering scheme. Hydrogen atoms have been omitted for clarity. Symmetry transformation, ^{a} = 1-x, -y, 1-z. (b) Asymmetric unit of the complex. Selected bond lengths (Å): Cu(1)–O(11) = 1.924(3), Cu(1)–N(1) = 1.961(4), Cu(1)–N(19) = 1.947(4), Cu(1)–N(22) = 2.036(4), Cu(1)–O(11)^{a} = 2.770(3), Cu(1)–S(1)^{b} = 2.886(14). Symmetry transformation ^{a} = 1-x,-y,1-z; ^{b} = 3/2-x,1/2+y,z.

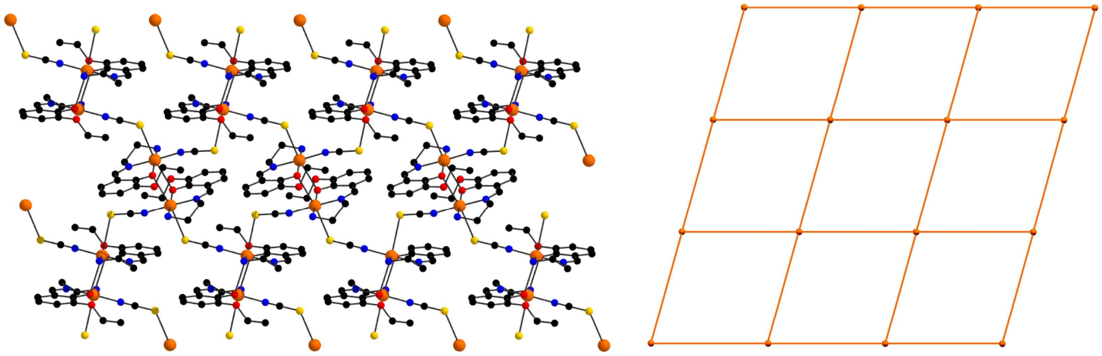

(a)

(b)

Fig. 2: (a) Two-dimensional layer of the complex. Ethyl groups and hydrogen atoms are omitted for clarity. (b) A perspective view of (4,4) Square grid topology of the complex.

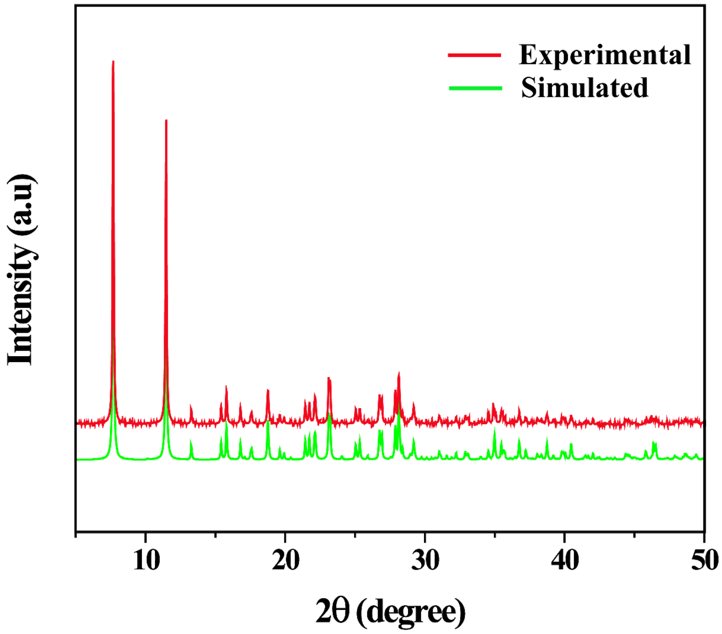

Fig. 3: Experimental and simulated powder XRD patterns of the complex confirming the purity of bulk material.

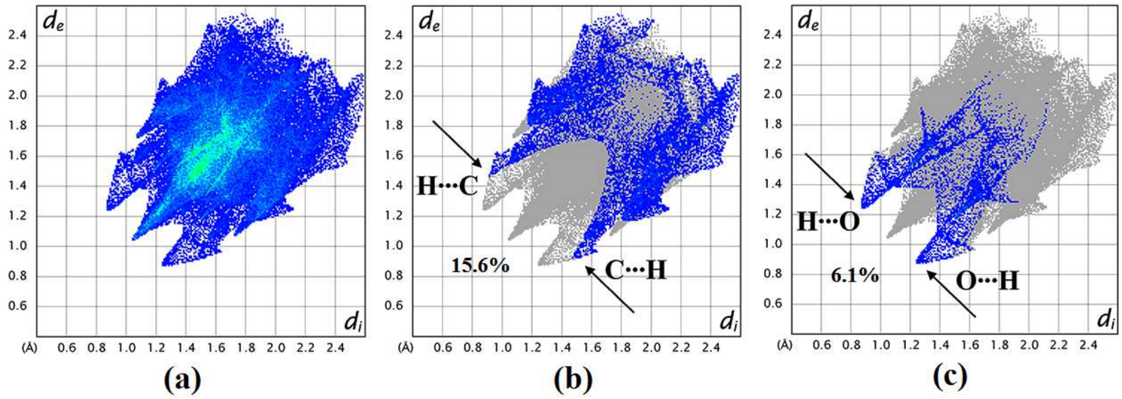

Fig. 4: (a) 2D fingerprint plot (full); (b) 2D fingerprint plot with C···H/H···C interactions (c) 2D fingerprint plot with O···H/H···O interactions highlighted in color.

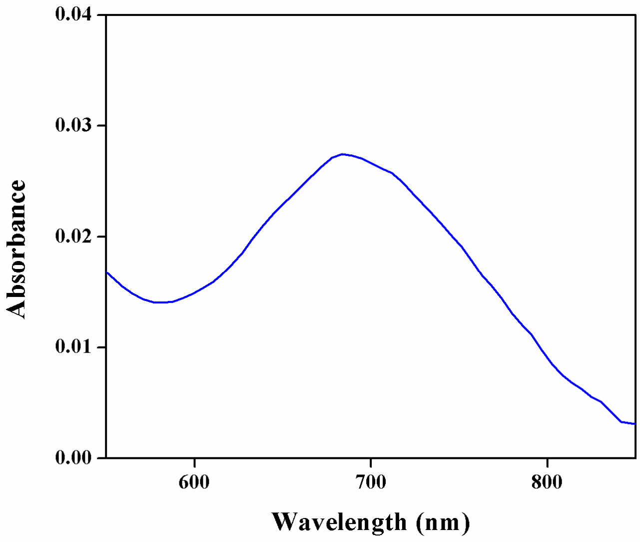

Fig. 5: Electronic spectrum of the complex in the visible region.

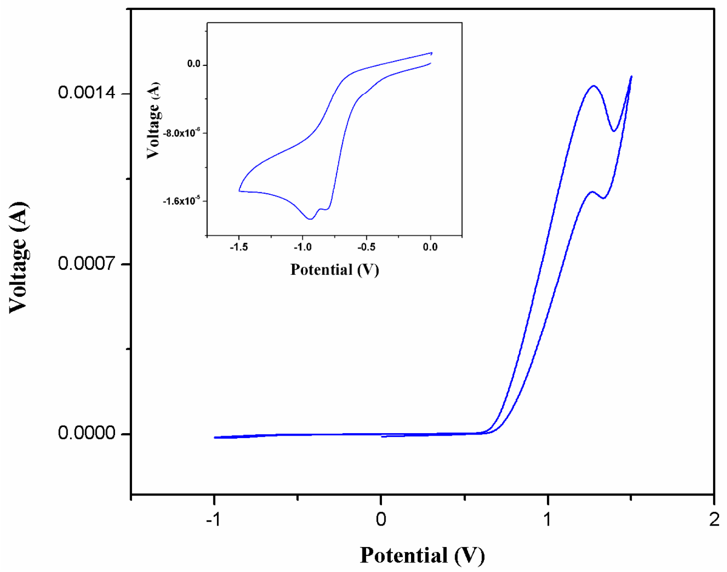

Fig. 6: Cyclic voltammogram of the complex in acetonitrile.

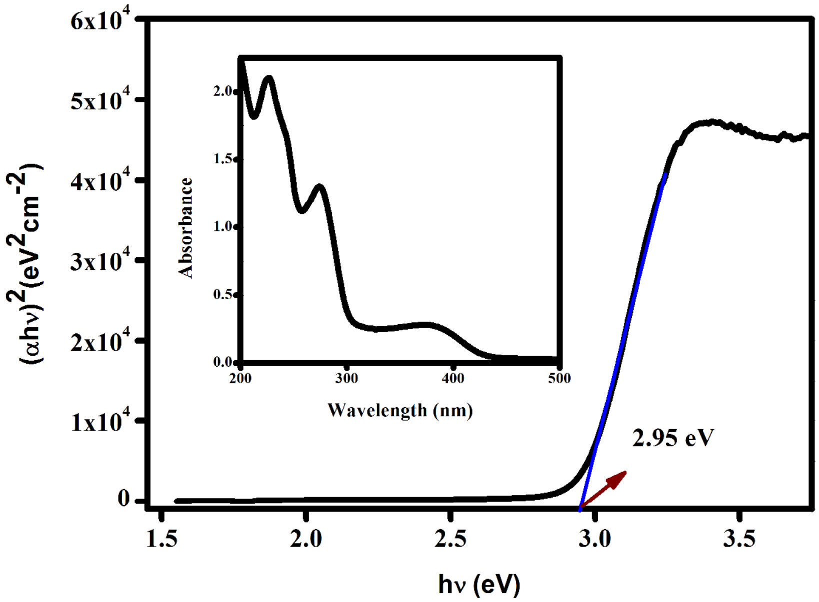

Fig. 7: Tauc's plot and UV-vis absorption spectra (inset)

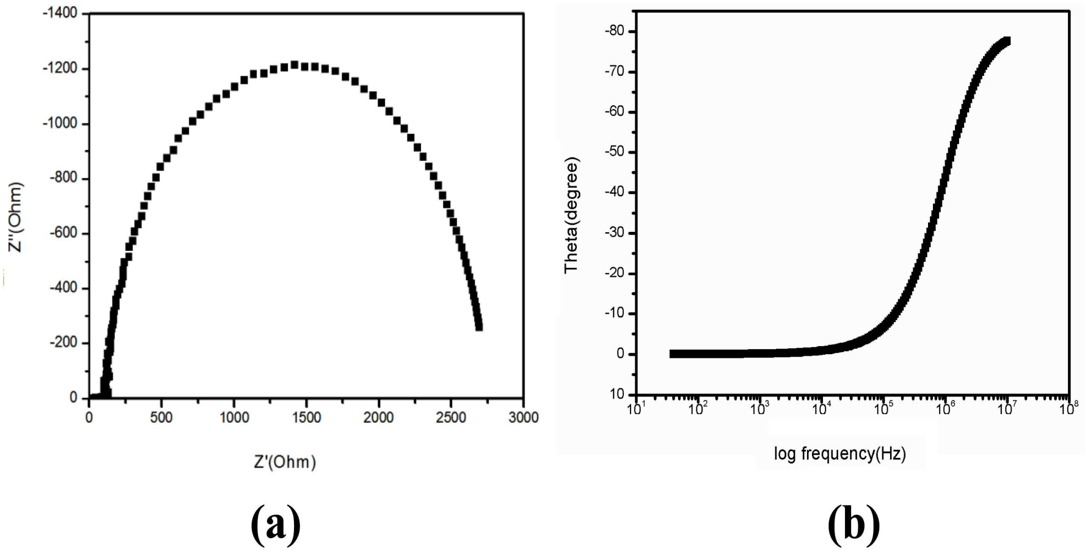

Fig. 8: (a) Nyquist plot of the complex. (b) Bode plot of the complex.

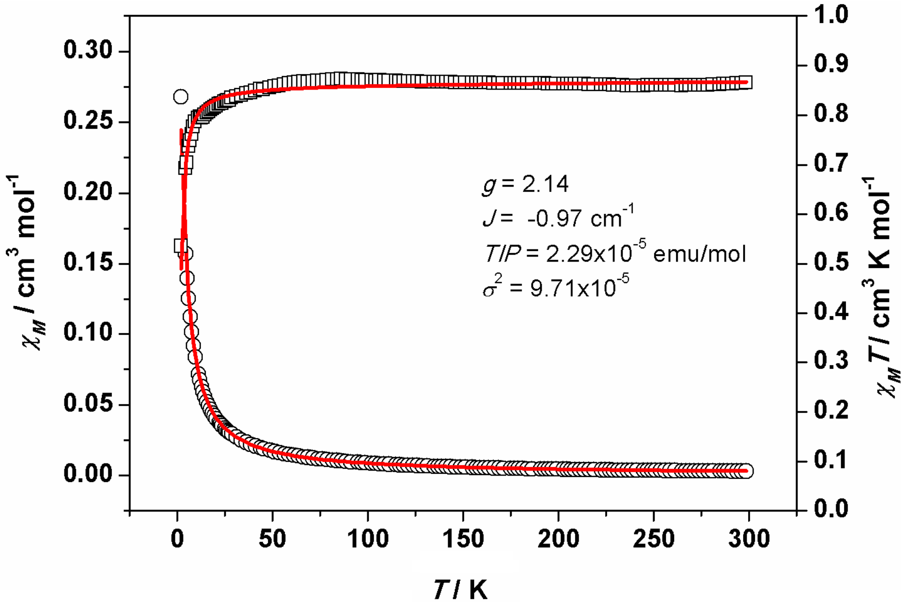

Fig. 9: Magnetic susceptibility (open circles) and $\chi_M T$ (open squares) versus temperature for the complex. Solid lines indicate the best fit obtained using the model indicated in the text.

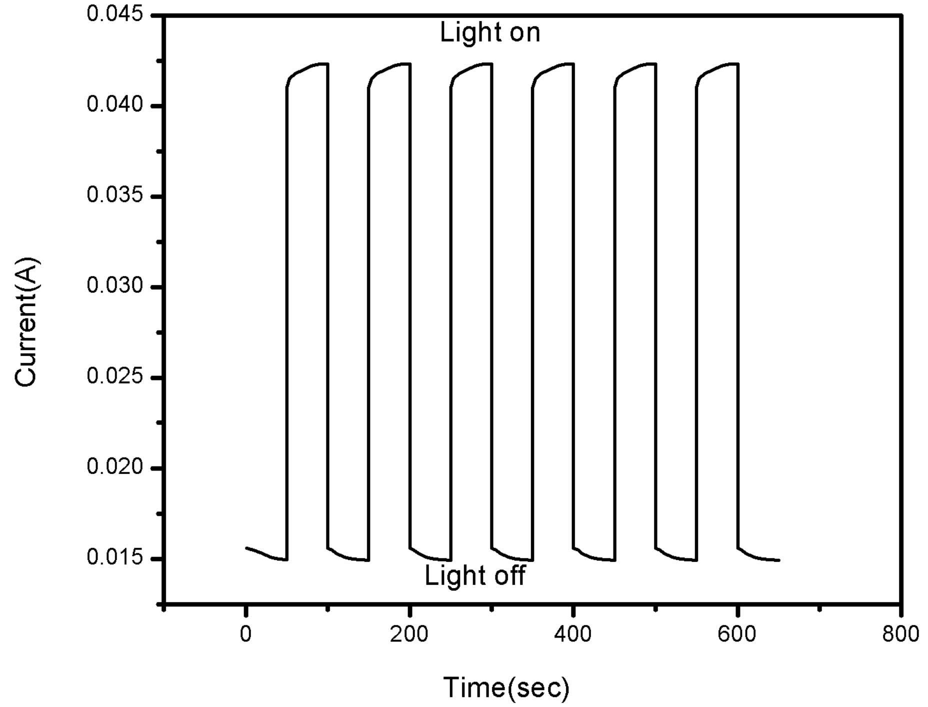

Fig. 10: Transient photocurrent response of the complex.

For Table of Contents Use Only

A semiconducting copper(II) Metal–Organic Framework with (4,4) square grid topology: Synthesis, characterization and application in the formation of a photo-switch

Samim Khan, Soumi Halder, Partha Pratim Ray, Santiago Herrero, Rodrigo González-Prieto, Michael G. B. Drew and Shouvik Chattopadhyay

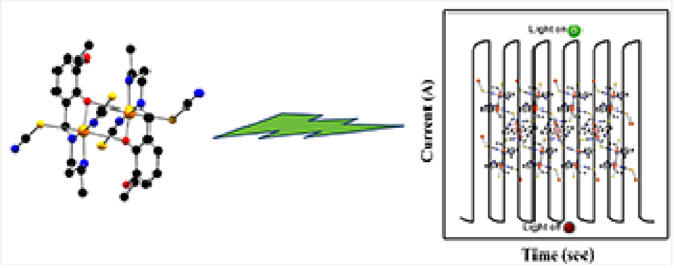

A MOF composed of phenoxo bridged dinuclear copper(II) node and end-to-end thiocyanate linker has been synthesized and characterized. The complex shows increase in conductivity when illuminated with visible light.